



crystals

IMPACT
FACTOR
2.4

CITESCORE
4.2

Article

Synthesis and Computational Investigations of New Thioether/Azomethine Liquid Crystal Derivatives

Alaa Z. Omar, Mohamed A. El-Atawy, Mai S. Alsubaie, Mohammed L. Alazmi, Hoda A. Ahmed and Ezzat A. Hamed

Special Issue

Schiff Base Derivatives: Synthesis, Crystal Structure, Applications, Hirshfeld Surface Analysis

Edited by




Prof. Dr. Saied M. Soliman, Prof. Dr. Assem Barakat and Prof. Dr. Ayman El-Faham



<https://doi.org/10.3390/cryst13030378>

Article

Synthesis and Computational Investigations of New Thioether/Azomethine Liquid Crystal Derivatives

Alaa Z. Omar ¹, Mohamed A. El-Atawy ^{1,2}, Mai S. Alsubaie ¹, Mohammed L. Alazmi ¹, Hoda A. Ahmed ^{3,*}
and Ezzat A. Hamed ^{1,*}

¹ Chemistry Department, Faculty of Science, Alexandria University, P.O. Box 426 Ibrahemia, Alexandria 21321, Egypt

² Chemistry Department, Faculty of Science, Taibah University, Yanbu 46423, Saudi Arabia

³ Department of Chemistry, Faculty of Science, Cairo University, Giza 12613, Egypt

* Correspondence: ahoda@sci.cu.edu.eg (H.A.A.); ezzat.awad@alexu.edu.eg (E.A.H.)

Abstract: Methylthio moiety was observed to alter the mesomorphic features of rod-like Schiff-base-derived liquid crystalline materials. For this purpose, a new series of (*E*)-4-(alkoxy)-*N*-(4-(methylthio)benzylidene)aniline (**I_n**) liquid crystals were synthesized and examined using experimental and computational approaches. The compounds in the series differ from each other in the terminal alkoxy chain length that is attached to one end of the aromatic core. Various spectroscopic methods were used to verify the molecular structures of the produced derivatives. All compounds were checked for correct chemical structures using elemental analysis, FT-IR, ¹H-NMR, and ¹³C-NMR. Both a polarized optical microscope (POM) and a differential scanning calorimeter (DSC) were used in order to study the behavior of liquid crystals. Both tested compounds **I₆** and **I₈** have monotropic nematogenic properties while the longer chain derivative **I₁₆** shows non-mesomorphic behavior. Computational studies were carried out using density functional theory (DFT) calculations to validate the experimental results. All of the analyzed compounds had their reactivity characteristics, dipole moments, and polarizability explained. Finally, in order to determine the chemical shape-mesomorphic property relationship, the present examined series was compared to other structurally comparable homologues.

Keywords: thioether liquid crystal; Schiff base; nematic phase; DFT; (*E*)-4-(alkoxy)-*N*-(4-(methylthio)benzylidene)aniline



Citation: Omar, A.Z.; El-Atawy, M.A.; Alsubaie, M.S.; Alazmi, M.L.; Ahmed, H.A.; Hamed, E.A. Synthesis and Computational Investigations of New Thioether/Azomethine Liquid Crystal Derivatives. *Crystals* **2023**, *13*, 378. <https://doi.org/10.3390/cryst13030378>

Academic Editor: Borislav Angelov

Received: 17 January 2023

Revised: 12 February 2023

Accepted: 21 February 2023

Published: 23 February 2023



Copyright: © 2023 by the authors. Licensee MDPI, Basel, Switzerland. This article is an open access article distributed under the terms and conditions of the Creative Commons Attribution (CC BY) license (<https://creativecommons.org/licenses/by/4.0/>).

1. Introduction

Liquid crystals (LCs), are an interesting subclass of soft matter, with features that lie between those of solid crystals and liquids [1]. They have attracted a great deal of attention due to their incredibly useful and interesting uses in a number of scientific areas, including sunlight-driven polymer actuators [2], Pancharatnam–Berry (PB) microlenses [3], biosensors [4], organic field effect transistors (OFETs) [5], liquid crystal elastomers [6], photovoltaics [7], and telecommunications [8]. Designing and manufacturing new, inexpensive liquid crystalline materials with great thermal stability and a large mesophase temperature range will always be a challenge. One of the most effective ways to develop novel, affordable LC materials with specific properties has turned out to be chemically changing geometry.

Even relatively few alterations to molecular geometry of the molecule, such as the inclusion of heteroatoms or the presence of various lateral substituted atoms or groups [9], can result in substantial modification in its mesomorphic behavior. Different types and classes of substituents with different polarities have been repeatedly incorporated into different LC structures, in order to modify the molecular geometry, conformational preferences, the transition temperature, the mesomorphic properties, and some other crucial

physical properties that are necessary for designing and developing new low-cost LC materials with improved properties suitable for display technologies. The development of new technologies, such as liquid crystal lasers and lenses, could be enhanced by nematogens with a high birefringence, which are already being used to improve LCD displays. Accordingly, nematogens that contain terminal alkylthio chains have high birefringence values, because the sulfur atom in their structures is highly polarizable. [10,11].

Schiff bases are a prominent group of chemical compounds that include the imine ($-C=N-$) connection. Schiff bases have numerous potential uses in a range of industries, including catalysis [12], corrosion chemistry [13], pharmaceuticals [14], and photochromism [15]. Since they are able to preserve a linear geometry, high stability, and the polarity of their imine linkages, they serve as a strong core structure that allows mesophase formation [16]. All Schiff base characteristics have been extensively investigated for their fascinating liquid crystalline behavior [17]. Since the discovery of LCs, many studies have been conducted on compounds containing heteroatoms (N, O, or S). Due to the polarizability of heteroatoms, their incorporation into LC molecules has a significant impact on the molecular geometry, phase transitions, mesomorphic properties, dielectric properties, and thermal stability, producing advanced functional materials with intriguing mesomorphic properties. Moreover, the incorporation of the alkylthio group with an imine linkage significantly challenges our knowledge of the relationship between molecular structure and liquid crystalline behavior. Using differential thermal analysis (DSC) and polarization optical microscopy (POM) in the course of an experimental investigation, the thermal and mesomorphic behavior of the novel series has been characterized. Theoretically, these findings will be explored within the context of density field theory (DFT). Some of our research focus is on integrating experimentally established values with theoretical models for estimating the effects of molecular geometry confirmation on the distinctive attributes. The multiple optical factors interact with one another, demanding stimulated knowledge of both the LCs' molecular geometries and orbital energies. Additionally, DFT is an effective method for easily acquiring insight into the characteristics of the molecule.

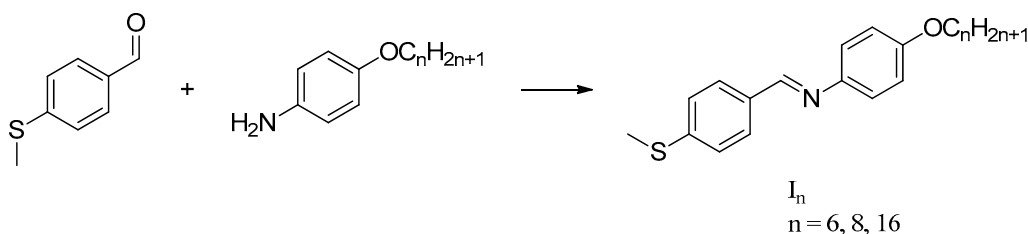
The aim of the present work is to synthesize new Schiff-base-derived LCs and to investigate the influence of the terminal methylthio group on the phase behavior of the resulting derivatives. Therefore, series of LC compounds (I_n), namely, ((*E*)-4-(alkoxy)-*N*-(4-(methylthio)benzylidene)aniline, were synthesized. Compounds in the series differ from each other in the length of the terminal alkoxy chain connected to an end, where hexyloxy, octyloxy, and hexadecyloxy chains are used, while the other end is connected to the methylthio group. The liquid crystal investigations of all synthesized compounds were carried out using DSC and POM. The theoretical parameters were investigated using DFT calculations. These calculations are also used to demonstrate the terminal groups affect mesomorphic characteristics.

2. Results and Discussion

2.1. Chemistry

Schiff bases I_n were prepared via direct condensation reaction between 4-methylthiobenzaldehyde with alkyloxy anilines, as demonstrated in Scheme 1. Molecular formulas and structures of I_n were verified using elemental analysis, FT-IR measurements, and NMR spectroscopy. The spectroscopic findings match the expected structures. All of the synthesized compounds display the alkyl aliphatic protons abundance when analyzed by Fourier-transform infrared (FT-IR) and nuclear magnetic resonance (NMR) spectroscopy. Infrared spectrum of I_n shows absorption peaks in the region $2917\text{--}2963\text{ cm}^{-1}$ that can be ascribed to the typical absorption for aliphatic C-H stretching. Furthermore, the azomethine group shows an absorption band in the region $1619\text{--}1657\text{ cm}^{-1}$, which distinguishes the amine group stretching. In the $^1\text{H-NMR}$ spectrums, the aliphatic side chain protons reveal peaks at the chemical shift from 0.89 to 3.99 ppm. Moreover, their equivalent carbons show peaks in the region 14.14–68.32 ppm in $^{13}\text{C-NMR}$. Moreover, the unsaturated aromatic moiety is identified in both carbon and proton NMR spectra. Thus, protons of the aromatic

rings show four doublet peaks in the downfield region from 6.94 to 7.85 ppm in proton NMR, whereas the carbon NMR spectrum displays downfield peaks in the region 114.99 to 157.80 ppm, and these attributed to the carbons of the aromatic ring. Consequently, the highly deshielded signal at 157.80 ppm is ascribed to the non-hydrogenated aromatic carbon that directly connects to the alkoxy side chain.



Scheme 1. Synthesis of (*E*)-4-(alkoxy)-*N*-(4-(methylthio)benzylidene)aniline (I_n).

Furthermore, the existence of the doubly bonded imine group (Schiff base) is established by NMR. Therefore, the H-NMR spectra show a singlet peak in the region δ 8.44–8.59 ppm that matches the imine proton. Moreover, ^{13}C -NMR displays a downfield peak near ≈ 158 ppm, which corresponds to the imine unsaturated carbon. Recently, both elemental analysis and MS provided further confirmation for their molecular formula and structures.

2.2. Liquid Crystalline Properties

Figure 1 displays the DSC thermograms of typical compounds I_6 and I_8 during heating and cooling scans. It is evident that compounds display only one endotherm peak that is typical of crystal–isotropic transitions following heating. Both I_6 and I_8 compounds display two transition temperatures during the cooling cycle. The POM measurements show textures that support the formation of N mesophases (Figure 2). While *n*-hexyloxy and *n*-octyloxy derivatives show a nematic phase under a POM, *n*-hexadecyloxy derivatives do not show any liquid crystal phase. This demonstrates that, depending on the terminal chain length, these compounds possess monotropic characteristics with a mono-morphic phase. Table 1 provides a summary of the details on the transition temperatures and related enthalpy of all studied homologues series (I_n). To determine the effect of the terminal alkoxy chain length on the mesophase behavior, the transition temperatures of all the examined derivatives are graphically displayed in Figure 3.

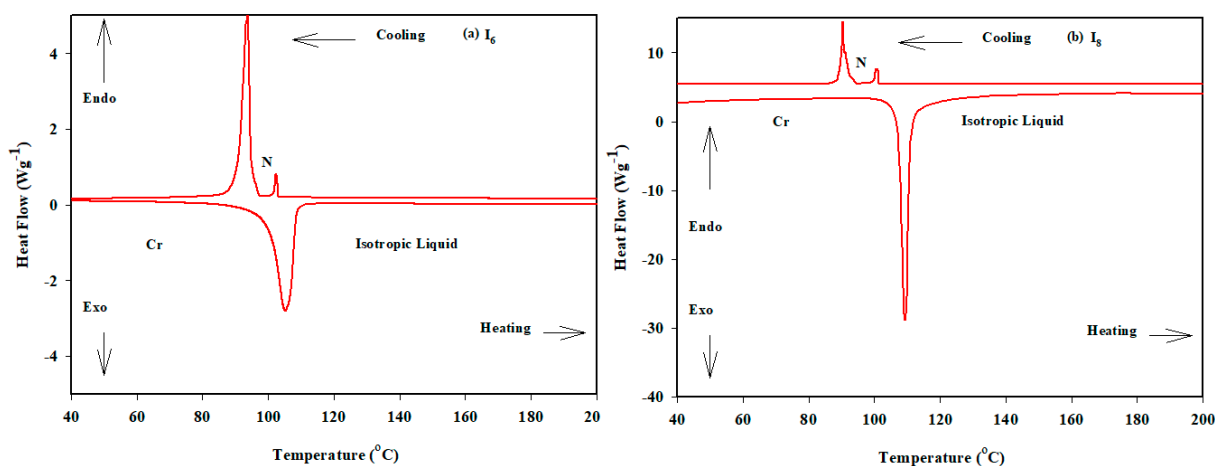


Figure 1. DSC thermograms of (a) I_6 and (b) I_8 observed from second heating/cooling at a rate of $\pm 10^\circ \text{C}$.



Figure 2. Nematic texture of I_8 derivative upon cooling round at 99°C under POM.

Table 1. Transition temperatures ($^\circ\text{C}$), enthalpy in kJ/mol, and normalized entropy of transitions for series I_n .

Comp.	$T_{\text{Cr-N}}$	$\Delta H_{\text{Cr-N}}$	$T_{\text{N-I}}$	$\Delta H_{\text{N-I}}$	$\Delta S_{\text{N-I}}$
I_6	105.3	57.14	101.2 *	0.69	0.22
I_8	109.2	49.75	101.4 *	1.29	0.41
I_{16}	113.1	60.69	-	-	-

The phase transition from solid to nematic is denoted by the notation Cr-N, while the phase transfer from nematic to isotropic is denoted by the notation N-I. * Monotropic phase.

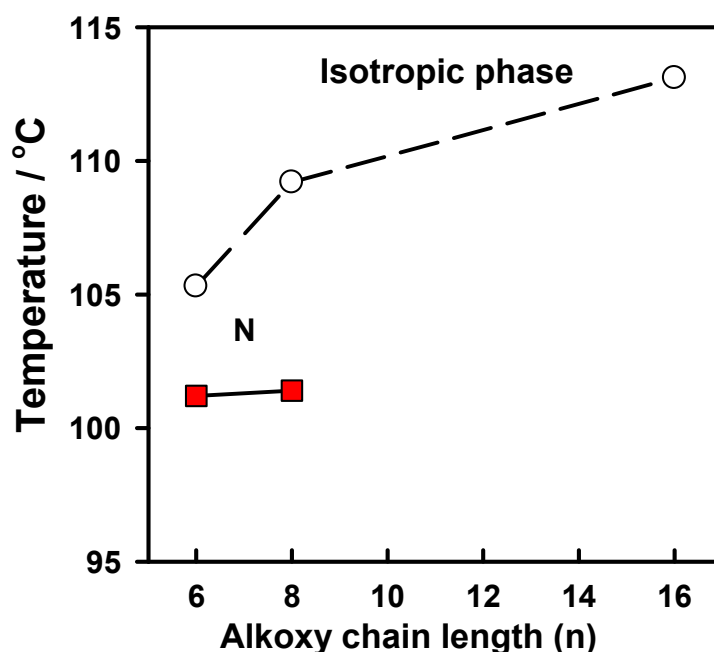


Figure 3. Graphical DSC transitions for derivatives I_n .

Data from Table 1 and Figure 3 show that as the length of the alkoxy chain increases from $n = 6$ to 16, the melting temperatures of the produced derivatives also increases. The melting point increases as the polarizability of the compounds within the same series increases. Additionally, every member of the homologous series is monotropic, has a limited temperature mesomorphic range, and has low mesophase thermal stability. The shortest terminal chain compound ($n = 6$) is monomorphic and purely nematogenic, exhibiting a monotropic N phase. The $\text{C}_8\text{H}_{17}\text{O}$ derivative (I_8) also exhibits a monotropic N phase. The I-N transition phase stability upon cooling is mostly the same for both compounds I_6 and I_8 , due to the difference in terminal chain length in two CH_2 units. The compound with longest chain length (I_{16}) is found to be non-mesomorphic. Only two members ($n = 6, 8$) of

the prepared group display liquid crystalline behavior. Despite how unusual this pattern is, it remains interesting to find out why the longer chain ($n = 16$) is non-mesomorphic. The lower tendency in the thermal transition of the N phase is caused by the reduction in the rigid mesogenic core. However, as the length of the alkoxy chain increases, the N phase range reduces until it disappears at $n = 16$. This possibly could be explained based on the intensification of the Van der Waals forces that exist between lengthy alkoxy chains, which causes their interweaving and produces lamellar packing, which disrupts the N phase.

According to the aforementioned findings, crucial elements such the polarizability, polarity of the substituent groups, stiffness, aspect ratio, and molecular architecture are often responsible for the stability of the generated mesophase. These factors have varying degrees of influence on how the mesophase behaves. It is well-known that an increase in the polarity and/or polarizability of the mesogenic core of a particular mesomorphic compound, which is influenced by the polarity of the substituent that consequently affects the polarity of the entire molecular structure, increases the stability of a mesophase of that compound. The estimated entropy changes of mesophase transitions ($\Delta S/R$) for the substances under investigation are displayed in Table 1. The ($\Delta S/R$) related to the N transition is found in small magnitudes for both liquid crystalline derivatives **I**₆ and **I**₈. The slight promotion of molecular biaxiality by the azomethine linkage group [18,19], however, may be the reason of the minor values observed in both members **I**₆ and **I**₈.

2.3. Effect of the Methylthio Group on the Mesomorphic Behavior

The present group was compared to previously synthesized, structurally comparable compounds in order to determine the relationship between chemical structure and mesomorphic properties. A homologous group of azomethine mesogens, including *N*-4-fluorobenzylidene-4-(alkyloxy)benzenamine (**II**_{*n*}, Figure 4), was recently reported [20]. Depending on the terminal alkoxy chains length, all the homologues previously synthesized exhibited monotropic smectogenic properties with different thermal stability [20]. The mesomorphic properties of that terminal fluorinated series (**II**_{*n*}) were compared with our prepared series **I**_{*n*} to examine the impact of the terminal polar group on the mesomorphic behavior, and the mesomorphic features of that terminal fluoro group were compared with our synthesized methylthio series, **I**_{*n*}.

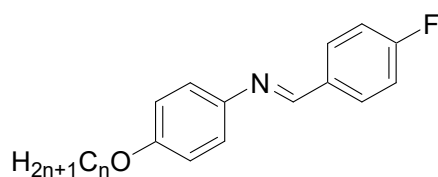
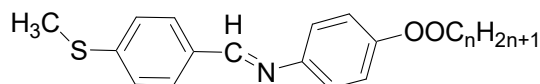


Figure 4. *N*-4-fluorobenzylidene-4-(alkyloxy)benzenamine, **II**_{*n*}.

Compounds **II**_{*n*} differ from our group **I**_{*n*} only in the terminal aromatic ring of their molecules; the latter have F substituent at the terminal benzene nucleus while the former have a methylthio group there. It was reported that compounds **II**_{*n*} are fully smectogenic, possessing purely smectic A phases, while **I**_{*n*} are purely nematogenic, except the **I**₁₆ derivative. A comparison between our current group **I**_{*n*} and **II**_{*n*} is made in order to examine the impact of the terminal methylthio group insertion into the terminal ring of the molecule on the formation, nature, and stability of the mesomorphic behavior of compounds. The elevated molecular dipole moment of the mesogenic core, which is mostly based on the location of the polar group, determines the nature and stability of the mesophase that is produced. Additionally, the smectic A molecular packing is disrupted by the insertion of the methylthio group into the para position with regard to the imino group (**I**_{*n*}), leading to purely nematic phases for $n = 6$ and 8 carbons. The location and/or orientation of the methylthio group have a major role in determining the type and stability of the mesophase formation.

In another work [21], 4-(methylthio)benzylidene-4'-n-alkanoyloxyanilines (**III_n**, Figure 5) were reported, and their mesomorphism investigated. It was found that the n-hexanoyloxy (**III₆**) and n-octanoyloxy (**III₈**) derivatives exhibited monotropic nematic phase, while the n-hexadecanoyloxy (**III₁₆**) derivative showed non-mesomorphic behavior. The mesophase was disrupted for the longer terminal chain component, and the intermolecular interactions within the molecule were thought to be affected by the length of the molecular shape.



III_n

$n = 6, 8, 16$

Figure 5. 4-(Methylthio)benzylidene-4'-n-alkanoyloxyanilines, **III_n**.

2.4. DFT Study

2.4.1. Optimized Geometry and Thermal Parameters

A compound's geometry is an essential characteristic that affects how the molecule behaves in other aspects. In order to find the most stable geometry, the optimum geometrical structures of series **I_n** were adopted. The estimated quantum chemical parameters were correlated computationally using the DFT method for all azomethine derivatives. Using the DFT method with the B3LYP 6-311G(d,p) basis set, DFT calculations were performed in the gas phase. Each optimized geometrical structure, shown in Figure 6, was stable, and this is acceptable due to the lack of the imaginary frequency. Table 2 provides a summary of the computed quantum thermal parameters, zero-point energy, polarizability, and dipole moment of all investigated compounds, **I_n**.

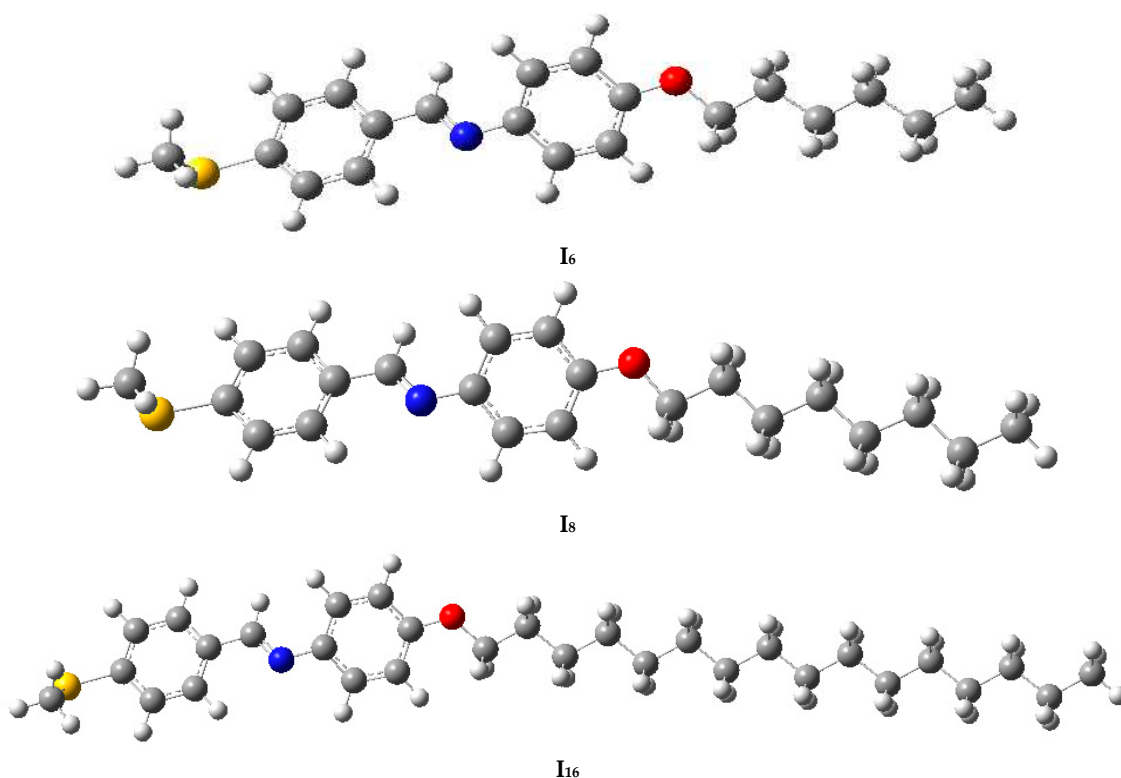


Figure 6. The optimized geometries of the investigated compounds, **I_n**.

Table 2. Estimated thermal parameters, polarizability, and dipole moment for investigated series, I_n .

Compound	ZPE (Kcal/Mol)	Thermal Energy (Kcal/Mol)	Enthalpy (Kcal/Mol)	Gibbs Free Energy (Kcal/Mol)	Entropy (Cal mol.k)	Polarizability (α) Bohr ³	Dipole Moment(D)
I_6	255.2745	270.4004	270.9928	218.4428	176.2572	295.8240	2.9016
I_8	291.0420	307.9067	308.4997	251.3037	191.83846	319.9326	2.8768
I_{16}	437.6267	461.1987	461.7917	387.5484	249.0150	396.9743	2.8560

The length of the alkyl chain was discovered to affect the calculated thermodynamic parameters and zero-point energy of compounds I_n [22,23]. They were expected to increase as the alkyl chain length in series I_n increased. As seen in compound I_{16} , the longer nonpolar moiety provides high thermal stability.

The DFT outcomes show that the dipole moment in series I_n decreases with increasing the non-polar part of alkyl chain, indicating that the length of alkyl moiety has a significant impact on the reactivity of investigated compounds. The polarizability of a molecule is determined by the responsiveness of the electron cloud in a molecular system to the approach of a charge. Larger compounds are more polarizable. Accordingly, it is found that compound I_{16} has the highest polarizability due to the large size.

2.4.2. Frontier Molecular Orbitals

Frontier molecular orbitals (FMO) are defined as the highest occupied (HOMO) and lowest unoccupied (LUMO) molecular orbitals. The LUMO has a capacity for accepting electrons, making it an electron acceptor, whereas the HOMO is an electron donor. An increase in HOMO energy and a decrease in LUMO energy generally results in an increase in a molecule's binding power. Using the DFT method with the B3LYP 6-311G(d,p) basis set, the energies of the HOMOs and LUMOs of the compounds were determined, as shown in Table 3. The FMO shown in Figure 7 demonstrates that the distributions of HOMO and LUMO for series I_n are identical. In general, HOMO and LUMO electron clouds are evenly distributed over the two benzene rings, while HOMO located mainly on benzene ring come from alkoxy aniline, but LUMO in mainly distributed over arylidene moiety.

Table 3. Quantum chemical parameters based on optimized structures of the investigated compounds at B3LYP/6-311G(d,p) level of theory.

Parameter	I_6	I_8	I_{16}
E_{HOMO} (eV)	-0.2134	-0.2133	-0.2021
E_{LUMO} (eV)	-0.0708	-0.0707	-0.0604
ΔE (eV)	0.1426	0.1426	0.1417
IP (eV)	0.2134	0.2133	0.2021
EA (eV)	0.0708	0.0707	0.0604
χ (eV)	0.1421	0.1420	0.1313
μ (eV)	-0.1421	-0.1420	-0.1313
η (eV)	0.0713	0.0713	0.0708
σ (eV ⁻¹)	14.0292	14.0292	14.115
ω (eV)	0.1416	0.1415	0.1216

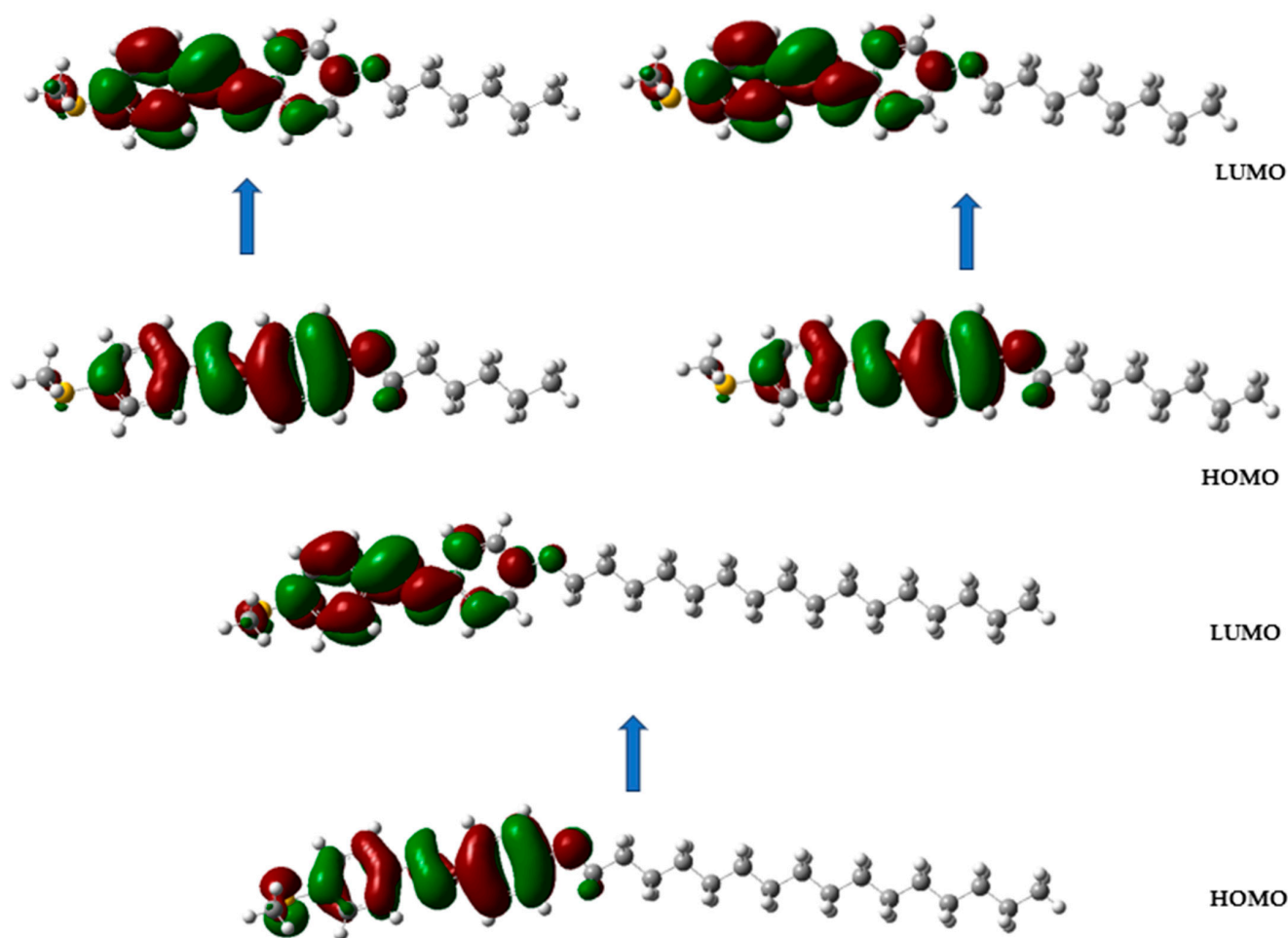


Figure 7. The frontier molecular orbitals for the compounds I_n calculated at the B3LYP/6-31+G(d,p) level of theory.

According to the FMO energy analysis, molecule I_{16} has greatest HOMO energy compared to the other compounds. However, I_6 has the highest LUMO energy. The chemical softness or hardness and chemical reactivity of the molecule are revealed by the energy gap between HOMO and LUMO. A soft molecule is one that has a small energy gap and exhibits strong chemical reactivity as well as stronger intermolecular interactions. Hard molecules are those that have a large energy gap and have higher thermal stabilities [24,25]. Consequently, the energy gap of compounds I_n is in the order of $I_6 = I_8 > I_{16}$.

2.4.3. Chemical Reactivity Descriptors

With the aid of DFT, the relationship between the stability, chemical reactivity, and molecular structure can be better understood using the global chemical reactivity descriptors. The calculation of many significant quantum chemical parameters, including electron affinity (EA), ionization potential (IP), chemical potential (μ), absolute electronegativity (χ), absolute softness (σ), absolute hardness (η), and electrophilicity index (ω) highly depends on the values of FMO. The larger values of the chemical hardness (η) reveal low molecular activity, while the softness parameter (σ) represents high molecular interactions. Furthermore, the interaction increases with increasing chemical potential.

Table 3 points out that, among series I_n , compound I_{16} has the highest reactivity based on all the computed parameters except E_{LUMO} , which predicts that compound I_6 should be the most reactive.

2.4.4. Molecular Electrostatic Potential (MEP)

It's crucial to establish the molecular electrostatic potential (MEP) in order to verify the information concerning the reactivity of series I_n . In terms of color shading, the MEP provides the fundamental details about the molecular size, shape, and essentially its positive, negative, and neutral electrostatic potentials. These could be used as a technique to forecast how the molecular structure of the substances relates to physicochemical properties. Red color denotes the negative potential, which is largely focused around oxygen and nitrogen atoms and is preferential for electrophilic attacks, while blue color denotes the positive potential, which is primarily localized on hydrogen atoms and shows the preferred sites for nucleophilic attacks. The MEP of the compounds I_n are shown in Figure 8, revealing that the shadowing of heteroatoms including oxygen, nitrogen, and sulfur atoms by a red cloud suggests a high electron density for these regions, whereas, the green cloud mainly distributed over the alkyl chains predicts low electron density but high electrostatic potential.

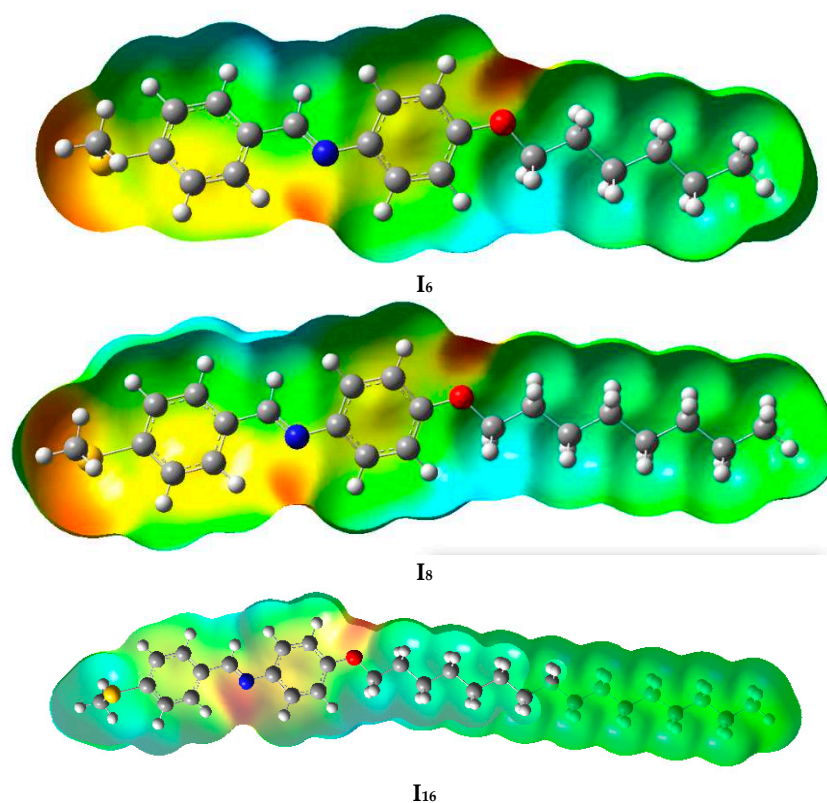


Figure 8. The molecular electrostatic potentials of the prepared I_n .

3. Experimental Section

3.1. Instruments and Apparatus

The purity of the prepared compounds was checked by thin-layer chromatography (TLC, E Merck, Rahway, NJ, USA). Melting points were determined by MEL-TEMP II melting point apparatus in open glass capillaries. The IR spectra were recorded as potassium bromide (KBr) discs on a Perkin–Elmer (Waltham, MA, USA) FT-IR (Fourier-transform infrared spectroscopy), Faculty of Science, Alexandria University. The NMR spectra were carried out at ambient temperature (~ 25 °C) on a (JEOL, Tokyo, Japan) 400 MHz spectrophotometer, NMR Unit, Faculty of Pharmacy, Mansoura University. Elemental analyses were analyzed at the Regional Center for Mycology and Biotechnology, Al-Azhar University, Cairo, Egypt. Mass spectrum were carried out on direct inlet part to mass analyzer in Thermo Scientific (Waltham, MA, USA) GCMS model ISQ at the Regional Center for Mycology and Biotechnology (RCMB), Al-Azhar University, Nasr City, Cairo. The mass

spectroscopy system was used to confirm the purity of the compounds as well as explore the characteristic fragmentation and the expected molecular weight.

Differential scanning calorimeter, TA instrument Co. Q20 (DSC; Des Plaines, IL, USA) was used for calorimetric measurements. The melting point and enthalpy of indium and lead were used for DSC calibration. Aluminum pans and (2–3 mg) sample amounts were used for DSC measurements investigation. Then, 30 mL/min nitrogen gas inert atmosphere and 10 °C/min heating rate were selected for all measurements and all transition were recorded from the second heating scan. The types of the mesophase texture were identified by a standard polarized optical microscope (POM, Wild, Germany) with Mettler FP82HT hot stage and the temperature controller was attached as thermocouple for temperature measurements. All recorded values were made twice, and the results have an accuracy of ± 0.2 °C for transition temperature.

3.2. General Method for Synthesis of (E)-4-(alkoxy)-N-(4-(methylthio)benzylidene)aniline **I_n**

To a stirred solution of 4-(methylthio)benzaldehyde (0.01 mol) in 10 mL absolute ethanol, alkoxy anilines (0.01 mol) were added and refluxed for 2–3 h. The reaction mixture was monitored by TLC. The crude products were filtered then washed by absolute ethanol.

(E)-4-(hexyloxy)-N-(4-(methylthio)benzylidene)aniline **I₆**

Colorless crystals, 3.04 g (93%) yield; m.p. 105–106 °C. IR (KBr): $\bar{\nu}$ 3092 ($S_P^2 = C-H$), 2930 ($S_P^3 -C-H$) and 1657 ($C=N$) cm^{-1} . 1H NMR (DMSO- d_6 , 400 MHz): δ 8.59 (s, 1H, CH=N), 7.84 (d, $J = 8.1$ Hz, 2H, Ar-H), 7.37 (d, $J = 8.1$ Hz, 2H, Ar-H), 7.27 (d, $J = 8.5$ Hz, 2H, Ar-H), 6.96 (d, $J = 8.5$ Hz, 2H, Ar-H), 3.98 (t, $J = 6.4$ Hz, 2H, OCH₂), 2.54 (s, 3H, SCH₃), 1.80–1.66 (m, 2H, CH₂), 1.47–1.40 (m, 2H, CH₂), 1.37–1.29 (m, 4H, 2 CH₂), and 0.89 (t, $J = 6.2$ Hz, 3H, CH₃) ppm. ^{13}C NMR (DMSO- d_6 , 126 MHz): δ 158.03, 157.78, 144.47, 142.75, 133.31, 129.25, 125.86, 122.84, 115.40, 68.13, 31.49, 29.16, 25.68, 22.56, 14.64, and 14.40 ppm. C₂₀H₂₅NOS requires: C, 73.33; H, 7.70; N, 4.27% found: C, 73.59; H, 7.84; N, 4.53%. MS M⁺ at m/z 327.07 (24%)

(E)-4-(octyloxy)-N-(4-(methylthio)benzylidene)aniline **I₈**

Colorless crystals, 3.19 g (90%) yield; m.p. 109 °C. IR (KBr): $\bar{\nu}$ 3037 ($S_P^2 = C-H$), 2963 ($S_P^3 -C-H$) and 1655 ($C=N$) cm^{-1} . 1H NMR (DMSO- d_6 , 400 MHz): δ 8.59 (s, 1H, CH=N), 7.85 (d, $J = 7.2$ Hz, 2H, Ar-H), 7.37 (d, $J = 8.0$ Hz, 2H, Ar-H), 7.28 (d, $J = 7.8$ Hz, 2H, Ar-H), 6.97 (d, $J = 8.3$ Hz, 2H, Ar-H), 3.98 (t, $J = 5.9$ Hz, 2H, OCH₂), 2.55 (s, 3H, SCH₃), 1.80–1.63 (m, 2H, CH₂), 1.49–1.37 (m, 2H), 1.32–1.24 (m, 8H, 4 CH₂), and 0.89 (t, $J = 9.9$ Hz, 3H, CH₃) ppm. ^{13}C NMR (DMSO- d_6 , 101 MHz): δ 158.07, 157.80, 144.47, 142.78, 133.33, 129.25, 125.86, 122.84, 115.44, 68.13, 31.72, 29.22, 29.18, 29.15, 26.01, 22.56, 14.64, and 14.45 ppm. C₂₂H₂₉NOS requires: C, 74.30; H, 8.23; N, 3.94% found: C, 74.58; H, 8.41; N, 4.18%. MS M⁺ at m/z 355.92 (23%)

(E)-4-(hexadecyloxy)-N-(4-(methylthio)benzylidene)aniline **I₁₆**

Colorless crystals, 4.10 g (88%) yield; m.p. 113 °C. IR (KBr): $\bar{\nu}$ 3038 ($S_P^2 = C-H$), 2917 ($S_P^3 -C-H$) and 1619 ($C=N$) cm^{-1} . 1H NMR (CDCl₃, 400 MHz): δ 8.44 (s, 1H, CH=N), 7.82 (d, $J = 8.2$ Hz, 2H, Ar-H), 7.32 (d, $J = 8.2$ Hz, 2H, Ar-H), 7.24 (d, $J = 8.6$ Hz, 2H, Ar-H), 6.94 (d, $J = 8.6$ Hz, 2H, Ar-H), 3.99 (t, $J = 6.5$ Hz, 1H, OCH₂), 2.55 (s, 3H, SCH₃), 1.91–1.73 (m, 2H, CH₂), 1.64 (s, 2H, CH₂), 1.56–1.40 (m, 2H, CH₂), 1.28 (s, 22H, 11CH₂), and 0.90 (t, $J = 6.5$ Hz, 3H, CH₃) ppm. ^{13}C NMR (CDCl₃, 101 MHz): δ 157.84, 157.51, 144.73, 142.59, 133.22, 128.87, 125.79, 122.15, 114.99, 68.32, 31.94, 29.93, 29.84, 29.80, 29.75, 29.71, 29.68, 29.62, 29.60, 29.43, 29.38, 29.33, 26.07, 22.71, 15.19, and 14.14 ppm. C₃₀H₄₅NOS requires: C, 7467.90 449.0729 (43%)

4. Conclusions

A new series of (E)-4-(alkoxy)-N-(4-(methylthio)benzylidene)aniline (**I_n**) liquid crystals were synthesized, and optically, as well as theoretically, investigated. Various spectroscopic methods were used to confirm their molecular structures. DSC and POM were used to study their mesomorphic behavior. Liquid crystalline phases were recorded depending

on the length of the terminal alkoxy chain. Moreover, both **I**₆ and **I**₈ derivatives exhibit monotropic mesomorphic ranges while the compound **I**₁₆ is non-mesomorphic. DFT results reveal that the dipole moment of the presented compounds decreases with increasing the non-polar part of alkyl chain, which may play role in the non-mesomorphic property that is observed for the longer chain derivative **I**₁₆.

Author Contributions: Methodology, A.Z.O., M.A.E.-A., M.S.A., M.L.A., H.A.A. and E.A.H.; Software, A.Z.O.; Formal analysis, M.S.A., H.A.A. and E.A.H.; Investigation, A.Z.O., M.A.E.-A., M.L.A. and H.A.A.; Resources, M.S.A. and M.L.A.; Writing—original draft, A.Z.O., M.A.E.-A., M.S.A., M.L.A., H.A.A. and E.A.H.; Writing—review & editing, M.A.E.-A., H.A.A. and E.A.H. All authors have read and agreed to the published version of the manuscript.

Funding: This research received no external funding.

Data Availability Statement: The data used for research described in this manuscript are available upon request from corresponding authors: ahoda@sci.cu.edu.eg (H.A.A.); ezzat.awad@alexu.edu.eg (E.A.H.)

Conflicts of Interest: The authors declare no conflict of interest.

References

1. Al-Zahrani, S.A.; Khan, M.T.; Jevtovic, V.; Masood, N.; Jeilani, Y.A.; Ahmed, H.A. Design of Liquid Crystal Materials Based on Palmitate, Oleate, and Linoleate Derivatives for Optoelectronic Applications. *Molecules* **2023**, *28*, 1744. [CrossRef]
2. Jiang, Z.C.; Xiao, Y.Y.; Tong, X.; Zhao, Y. Selective decrosslinking in liquid crystal polymer actuators for optical reconfiguration of origami and light-fueled locomotion. *Angew. Chem.* **2019**, *131*, 5386–5391. [CrossRef]
3. Jiang, M.; Guo, Y.; Yu, H.; Zhou, Z.; Turiv, T.; Lavrentovich, O.D.; Wei, Q.H. Low f-Number Diffraction-Limited Pancharatnam-Berry Microlenses Enabled by Plasmonic Photopatterning of Liquid Crystal Polymers. *Adv. Mater.* **2019**, *31*, 1808028. [CrossRef]
4. Zhang, C.; Nakano, K.; Nakamura, M.; Araoka, F.; Tajima, K.; Miyajima, D. Noncentrosymmetric Columnar Liquid Crystals with the Bulk Photovoltaic Effect for Organic Photodetectors. *J. Am. Chem. Soc.* **2020**, *142*, 3326–3330. [CrossRef]
5. Han, M.J.; Wei, D.; Kim, Y.H.; Ahn, H.; Shin, T.J.; Clark, N.A.; Walba, D.M.; Yoon, D.K. Highly oriented liquid crystal semiconductor for organic field-effect transistors. *ACS Cent. Sci.* **2018**, *4*, 1495–1502. [CrossRef] [PubMed]
6. Ula, S.W.; Traugott, N.A.; Volpe, R.H.; Patel, R.R.; Yu, K.; Yakacki, C.M. Liquid crystal elastomers: An introduction and review of emerging technologies. *Liq. Cryst. Rev.* **2018**, *6*, 78–107. [CrossRef]
7. Khalid, M.; Shanks, K.; Ghosh, A.; Tahir, A.; Sundaram, S.; Mallick, T.K. Temperature regulation of concentrating photovoltaic window using argon gas and polymer dispersed liquid crystal films. *Renew. Energy* **2021**, *164*, 96–108. [CrossRef]
8. Wilkinson, T. Applications of liquid crystals in telecommunications. In *Handbook of Liquid Crystals*; Wiley: New York, NY, USA, 2014; Volume 8, pp. 1–28.
9. Ahmed, H.A.; El-Atawy, M.A.; Alamro, F.S.; Al-Kadhi, N.S.; Alhaddad, O.A.; Omar, A.Z. Mesomorphic, Computational Investigations and Dyeing Applications of Laterally Substituted Dyes. *Molecules* **2022**, *27*, 8980. [CrossRef]
10. Arakawa, Y.; Inui, S.; Igawa, K.; Tsuji, H. Alkylthio- and alkyl-substituted asymmetric diphenyldiacetylene-based liquid crystals: Phase transitions, mesophase and single-crystal structures, and birefringence. *Liq. Cryst.* **2019**, *46*, 1621–1630. [CrossRef]
11. Arakawa, Y.; Sasaki, Y.; Haraguchi, N.; Itsuno, S.; Tsuji, H. Synthesis, phase transitions and birefringence of novel liquid crystalline 1, 4-phenylene bis (4-alkylthio benzoates) and insights into the cybotactic nematic behaviour. *Liq. Cryst.* **2018**, *45*, 821–830. [CrossRef]
12. Wang, L.; Hou, Y.; Zhong, X.; Hu, J.; Shi, F.; Mi, H. Preparation and catalytic performance of alginate-based Schiff Base. *Carbohydr. Polym.* **2019**, *208*, 42–49. [CrossRef] [PubMed]
13. Ansari, K.; Chauhan, D.S.; Quraishi, M.; Mazumder, M.A.; Singh, A. Chitosan Schiff base: An environmentally benign biological macromolecule as a new corrosion inhibitor for oil & gas industries. *Int. J. Biol. Macromol.* **2020**, *144*, 305–315. [PubMed]
14. Baumeister, J.E.; Reinig, K.M.; Barnes, C.L.; Kelley, S.P.; Jurisson, S.S. Technetium and rhenium Schiff base compounds for nuclear medicine: Syntheses of rhenium analogues to ^{99m}Tc-furifosmin. *Inorg. Chem.* **2018**, *57*, 12920–12933. [CrossRef] [PubMed]
15. Guo, S.; Liu, G.; Fan, C.; Pu, S. A new diarylethene-derived probe for colorimetric sensing of Cu (II) and fluorometric sensing of Cu (II) and Zn (II): Photochromism and high selectivity. *Sens. Actuators B: Chem.* **2018**, *266*, 603–613. [CrossRef]
16. Alhaddad, O.A.; Khushaim, M.S.; Gomha, S.M.; L Ahmed, H.A.; Naoum, M.M. Mesophase behavior of four ring ester/azomethine/ester liquid crystals in pure and mixed states. *Liquid Crystals* **2022**, *49*, 1395–1402. [CrossRef]
17. Al-Kadhi, N.S.; Alamro, F.S.; Popoola, S.A.; Gomha, S.M.; Bedowr, N.S.; Al-Juhani, S.S.; Ahmed, H.A. Novel Imidazole Liquid Crystals; Experimental and Computational Approaches. *Molecules* **2022**, *27*, 4607. [CrossRef]
18. Alamro, F.S.; Tolan, D.A.; El-Nahas, A.M.; Ahmed, H.A.; El-Atawy, M.A.; Al-Kadhi, N.S.; Shibl, M.F. Wide Nematogenic Azomethine/Ester Liquid Crystals Based on New Biphenyl Derivatives: Mesomorphic and Computational Studies. *Molecules* **2022**, *27*, 4150. [CrossRef]
19. Date, R.; Imrie, C.; Luckhurst, G.; Seddon, J. Smectogenic dimeric liquid crystals. The preparation and properties of the α , ω -bis (4-n-alkylanilinebenzylidene-4'-oxy) alkanes. *Liq. Cryst.* **1992**, *12*, 203–238. [CrossRef]

20. El-Atawy, M.A.; Naoum, M.M.; Al-Zahrani, S.A.; Ahmed, H.A. New nitro-laterally substituted azomethine derivatives; Synthesis, mesomorphic and computational characterizations. *Molecules* **2021**, *26*, 1927. [[CrossRef](#)]
21. Ha, S.-T.; Lee, T.-L.; Yeap, G.-Y.; Lin, H.-C.; Ito, M.M.; Subramaniam, R.T. Synthesis and Mesomorphic Properties of 4-(Methylthio) benzylidene-4'-n-alkanoyloxyanilines. *Asian J. Chem.* **2011**, *23*, 4609–4612.
22. Al-Zahrani, S.A.; Ahmed, H.A.; El-atawy, M.A.; Abu Al-Ola, K.A.; Omar, A.Z. Synthetic, Mesomorphic, and DFT Investigations of New Nematogenic Polar Naphthyl Benzoate Ester Derivatives. *Materials* **2021**, *14*, 2587. [[CrossRef](#)] [[PubMed](#)]
23. Alamro, F.S.; Ahmed, H.A.; El-Atawy, M.A.; Al-Zahrani, S.A.; Omar, A.Z. Induced Nematic Phase of New Synthesized Laterally Fluorinated Azo/Ester Derivatives. *Molecules* **2021**, *26*, 4546. [[CrossRef](#)] [[PubMed](#)]
24. Omar, A.Z.; Mahmoud, M.N.; El-Sadany, S.K.; Hamed, E.A.; El-atawy, M.A. A combined experimental and DFT investigation of mono azo thiobarbituric acid based chalcone disperse dyes. *Dye. Pigment.* **2021**, *185*, 108887. [[CrossRef](#)]
25. Omar, A.Z.; El-Rahman, M.A.; El-Sadany, S.K.; Hamed, E.A.; El-Atawy, M.A. Synthesis of novel bisazo disperse dyes: Spectroscopic characterization, DFT study and dyeing of polyester. *Dye. Pigment.* **2021**, *196*, 109831. [[CrossRef](#)]

Disclaimer/Publisher's Note: The statements, opinions and data contained in all publications are solely those of the individual author(s) and contributor(s) and not of MDPI and/or the editor(s). MDPI and/or the editor(s) disclaim responsibility for any injury to people or property resulting from any ideas, methods, instructions or products referred to in the content.